arXiv:1403.7031v1 [cond-mat.quant-gas] 27 Mar 2014

Itinerant ferromagnetism of repulsive spin-orbit coupled Fermi gases

Shang-Shun Zhang[1], Jinwu Ye[2,3], and Wu-Ming Liu[1]
[1] *Beijing National Laboratory for Condensed Matter Physics, Institute of Physics, Chinese Academy of Sciences, Beijing 100190, China*
[2] *Key Laboratory of Terahertz Optoelectronics, Ministry of Education, Department of Physics, Capital Normal University, Beijing 100048, China*
[3] *Department of Physics and Astronomy, Mississippi State University, MS 39762, USA*
(Dated: March 28, 2014)

We investigate the itinerant ferromagnetism of repulsive ultra-cold Fermi gases with spin-orbit coupling. We find the critical interaction strength for ferromagnetic transition is apparently suppressed due to the flat-band structure at the bottom of the single-particle spectrum, which is benefit to experimental observation of itinerant ferromagnetism. Properties in both the normal and ferromagnetic side show up essentially new features due to the interplay of spin-orbit coupling, interaction and magnetic order. Critical behaviors of physical observables near the ferromagnetic transition point are investigated, which generalized the Hertz-Millis theory on traditional ferromagnetic transition. Finally, we discussed the experimental study of these phenomena in present ultra-cold platform.

Introduction— Ultra-cold atom physics has received a rapid development in recent years. Due to its highly tunability, people are able to design various clean systems with tunable parameters [1–3]. The absence of disorders, lattice oscillations existed in condensed matter systems makes the experimental study of theoretical models a possible issue. Spin-orbit coupling (SOC) exists widely in nature and gives rise to various exotic new states of matters, such as topological insulator and superconductor [4–8]. Recent years, people has devoted much attention to constructing and investigating SOC in the platform of cold-atom [9–13]. Various novel phenomena induced by SOC have been found due to its unique symmetry and single-particle spectrum [14–21]. Experimentally, people has realized 1D SOC, a combination of Rashba and Dresselhauss SOC, both in Bose and Fermi gas [11–13]. The experimental construction of the more interesting 2D and 3D Rashba SOC has also been proposed [22–24]. Due to its simplicity, the realization of arbitrary type of SOC is promising in recent years.

To the best of our knowledge, the study of SOC Fermi gas concentrated on the attracted interaction side, and dramatic SOC effects and new patterns of superfluid paring are discovered [20, 21]. However, the repulsive side has totally different and also intriguing physics, which depends on the unique structure of symmetry, Fermi surfaces and the single particle spectrum [25, 26]. The interplay between SOC, inter-atomic interaction and various symmetry breaking orders remains a mystery [27, 28]. Therefore, a systematic study of the repulsive SOC Fermi gas is desirable. Besides the rich physics, the repulsive SOC Fermi gas provides possibility to observe the long searching itinerant ferromagnetism [29–31], which is actually unobservable in ordinary Fermi gas due to the strong critical interaction strength [32, 33].

In this Letter, we investigated the itinerant ferromagnetism of repulsive SOC Fermi gas. We find the critical interaction strength for ferromagnetic transition is significantly weakened with increasing strength of SOC as a result of the enhanced density of states at Fermi surface, which is benefit to the observation of itinerant ferromagnetism in experiment. Properties in the normal and ferromagnetic side show up non-trivial features induced by SOC. New collective modes are found and the behaviors of them across the critical point are completely different from that of ordinary Fermi gas. Another important feature lies in that the total momentum of fermions with magnetic order is found to be nonzero, which breaks the orbital rotational symmetry and has important physical consequence, i.e., the appearance of two pseudo-Goldstone modes. We also analyzed the critical properties of the quantum critical point (QCP) via renormalization group method, which generalized the Hertz-Millis theory [34, 35] to the system in the presence of SOC. Given the rapid technical developments of cold atom, experimental study of repulsive SOC Fermi gas, such as the ground state magnetization and the critical behaviors of QCP, is promising [33, 36–39]. This work can be generalized to other types of SOC cases which are also interested in ultra-cold atom experiment.

General formulation.—We consider a repulsive two-component Fermi gas with isotropic spin orbit coupling, described by the Hamiltonian

$$\mathcal{H} = \sum_{\mathbf{k},\alpha,\beta} \Psi^{\dagger}_{\mathbf{k},\alpha} \left(\frac{\mathbf{k}^2}{2m} + \lambda \mathbf{k}\cdot\boldsymbol{\sigma} - \mu \right)_{\alpha,\beta} \Psi_{\mathbf{k},\beta} + g \sum_{\mathbf{k},\mathbf{p},\mathbf{q}} \Psi^{\dagger}_{\mathbf{k}+\mathbf{q},\uparrow} \Psi^{\dagger}_{\mathbf{p}-\mathbf{q},\downarrow} \Psi_{\mathbf{p},\downarrow} \Psi_{\mathbf{k},\uparrow}, \quad (1)$$

where λ is the SOC strength, which equals $k_{eff}/3m$ with k_{eff} characterizing the strength of magnetic field gradient in scheme [22–24], $g = 4\pi a_s/m$ with a_s the s-wave scattering length. The chemical potential μ is determined by the density of atoms self-consistently.

The interaction can be divided into the density and spin channel $\mathcal{H}_I = \frac{g}{8}\int d\mathbf{r}[\rho(\mathbf{r})^2 - \vec{S}(\mathbf{r})^2]$, where $\rho(\mathbf{r}) =$

$\Psi^\dagger\Psi(\mathbf{r})$ and $\vec{S}(\mathbf{r}) = \Psi^\dagger\vec{\sigma}\Psi(\mathbf{r})$. In presence of SOC, the density fluctuation is coupled with the spin fluctuation. We introduce the density-spin order $\phi_\mu, \mu = n, x, y, z$ to decouple the interaction term via a S-H transformation. After integrating out the fermionic field, we obtain the effective action for ϕ_μ

$$\mathcal{S}_H = \int d\mathbf{r} \int_0^{1/T} d\tau \frac{1}{2g}\phi_\mu^2 - \mathrm{Tr}\ln\left(-\mathcal{G}_0^{-1} + M\right), \quad (2)$$

where $\mathcal{G}_0^{-1} = -\partial_\tau - \mathcal{H}_0 + \mu$, $M = \frac{i}{2}\phi_n\sigma^0 + \frac{1}{2}\vec{\phi}\cdot\vec{\sigma}$. Away from the QCP of ferromagnetic transition, the fluctuation of order parameter ϕ_μ can be taken as a small quantity. Expanding Eq. (2) around the saddle point to the second order of ϕ_μ, we obtain $\mathcal{S}_H^{(2)} = 1/(2\beta V)\sum_{\mathbf{q},n}\mathcal{K}^{\mu\nu}\phi_\mu(-\mathbf{q}, -i\omega_n)\phi_\nu(\mathbf{q}, i\omega_n)$, where $\mathcal{K}^{\mu\nu} = \delta^{\mu\nu}/g - \bar{\chi}^{\mu\nu}(\mathbf{q}, i\omega_n)/4$, $\bar{\chi}^{\mu\nu}$ is related to the usual density and spin susceptibility $\chi^{\mu\nu}(\mathbf{q}, i\omega_n) = \langle s^\mu(\mathbf{q}, i\omega_n)s^\nu(-\mathbf{q}, -i\omega_n)\rangle$ via $\bar{\chi}^{00} = -\chi^{00}$, $\bar{\chi}^{0i} = i\chi^{0i}$, $\bar{\chi}^{ij} = \chi^{ij}$ with $i, j, = x, y, z$.

Collective modes.— Within the framework developed above, one can extract collective modes through the poles of density and spin correlation function. In the disordered side, we find one gapless mode, which is a coupled oscillation of density and longitudinal spin, and three branches of gapped modes corresponding to the spin fluctuations [26]. The dispersions for these modes are $\omega_{\mathbf{q}}^s = v_s q$, $\omega_{\mathbf{q}}^{T_1} = \omega_{\mathbf{q}}^{T_2} = \Delta_s + \beta_T q^2$, and $\omega_{\mathbf{q}}^L = \Delta_s + \beta_L q^2$. In weak SOC limit, the energy gaps Δ_s are shown to be proportional to SOC strength. For increasing strength of SOC, Δ_s approaches inter-band particle-hole continuum. And the velocity of zero sound v_s approaches the Fermi velocity. This suppression of v_s is due to the coupling of density and longitudinal spin fluctuation. The energy gaps at $\mathbf{q} = 0$ are degenerated because the original symmetry $[SO(3)_{orbit} \times SU(2)_{spin}]_D$ recovers to $SU(2)_{spin}$ when the orbital freedom vanishes as $\mathbf{q} = 0$. This degeneration is lifted for finite $\mathbf{q}$, i.e., $\beta_L \neq \beta_T$. One can find Δ_s vanishes for interaction strength larger than $g_s = 24\pi^2 k_R/m(k_2^2 - k_1^2)$, where $k_2 > k_1$ are the two Fermi momenta. This corresponds to instabilities in the collective modes channel. In the following section, we will show that magnetic ordering appears before these instabilities.

Stoner instability.—The normal state Fermi gas has a ferromagnetic instability when $\delta = \frac{1}{g_c} - \frac{\chi_0}{4} < 0$, i.e., the Stoner instability. Here χ_0 is the static spin susceptibility of 3D free Fermi gas with isotropic SOC, which is given by $\chi_0 = \frac{m}{6\pi^2}(\frac{k_1^2+k_2^2}{K} + \frac{k_2^2-k_1^2}{k_R})$, where $K = \sqrt{k_R^2 + 2m\mu}$ with $k_R = m\lambda$. We obtain the critical value $k_F a_s = F(\gamma)$ as shown in Fig. 1 (a), where k_F is the Fermi momentum without SOC for equal density, $\gamma = k_R/k_F$. $F(\gamma)$ has a maximum at $\gamma \simeq 0.63$, with chemical potential $\mu = -\frac{2}{3}E_R$ ($E_R = k_R^2/2m$), after which, $k_F a_s$ decreases quickly. This is a consequence of the flat band structure near the spectrum bottom, i.e., the degenerate surface

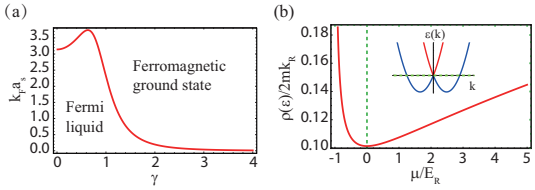

FIG. 1. (Color online) (a): Critical interaction strength $k_F a_s$ as a function of SOC strength $\gamma = k_R/k_F$. (b) Density of states $\rho(\epsilon)$ in units of $2mk_R$ as a function of chemical potential μ. The green dashed line denotes the chemical potential as shown by the inset.

$|\mathbf{k}| = k_R$. For strong SOC or dilute Fermi gas, the chemical potential μ approaches the bottom of the spectrum and the density of states at Fermi surface scales as $\frac{1}{\sqrt{\epsilon_F}}$ as in 1D Fermi gas (see Fig. 1 (b)). The effects of interaction is dramatically enhanced even if its strength is weak, which makes the realization of itinerant ferromagnetism in ultra-cold atom experiment more promising.

We find instability in the particle-hole channel happens first, before that in the collective mode channel because $g_s < g_c$. Hence, the most important low-energy and long wavelength quantum fluctuations occur in the limit $\mathbf{q} \to 0$ and $\omega/v_F q \to 0$. Naturally, one only need to expand the action of the critical fluctuations to the leading order of q and $y = \frac{|\omega_n|}{v_F q}$ to obtain the low energy effective action.

Hertz action of order parameters.—In the presence of SOC, it is convenient to define a helical basis $\hat{T}_1$, $\hat{T}_2$ and $\hat{L}$ which satisfy $\hat{T}_{1,2}\cdot\mathbf{q} = 0$ and $\hat{L} = \mathbf{q}/q$. In this basis, the propagators of the transverse spin mode $(\hat{T}_1\cdot\vec{s}, \hat{T}_2\cdot\vec{s})$ and longitudinal spin mode $(\hat{L}\cdot\vec{s})$ are decoupled.

The density-density fluctuation is NOT an order parameter, therefore non-critical across a magnetic phase transition, and one need to integrate it out. As noted above, the symmetry of SOC system $[SO(3)_{orbit} \times SU(2)_{spin}]_D$ recovers to $SU(2)$ symmetry in spin space when the orbital motion vanishes, i.e., zero momenta carried by the order parameter fluctuations. Therefore the most relevant interaction which carries zero momentum preserves the $SU(2)$ symmetry and has the form $\mathcal{S}_H^{int} = u\int d\mathbf{r}d\tau(\vec{\phi}^2)^2$ under spin σ_z basis. Finally, we obtain the low energy effective action

$$\mathcal{S}_H = \int\frac{d\mathbf{k}}{(2\pi)^3}T\sum_n \frac{1}{2}\mathcal{G}_s^{-1}\hat{P}_s^{ij}\phi_i\phi_j + u\int d\mathbf{r}d\tau(\vec{\phi}^2)^2, \quad (3)$$

where $\hat{P}_s^{ij} = \hat{n}_s^i\hat{n}_s^j$ ($\hat{n}_s = \hat{T}_1, \hat{T}_2, \hat{L}$) is the projection operator into the helical basis, $\mathcal{G}_{T_1}^{-1} = \mathcal{G}_{T_2}^{-1} = \delta + y + q^2$ and $\mathcal{G}_L^{-1} = \delta + \gamma_L y^2 + \alpha_L q^2$, are propagators of helical spin modes, where $y = |\omega_n|/v_F q$. The effective action of the critical fluctuations has the same form for $\mu > 0$ or $\mu < 0$. Note that the transverse propagator is the same as the ordinary Fermi gas without SOC with dynamical expo-

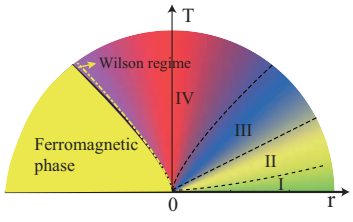

FIG. 2. (Color online) Finite temperature phase diagram of repulsive SOC Fermi gas as a function of control parameter r and temperature T. Transverse (Longitudinal) mode displays Fermi liquid behavior in regime I (I and II), and high temperature behavior in other regimes.

nent $z_T = 3$. The longitudinal mode behaves differently and has a dynamical exponent $z_L = 2$.

Critical behaviors at finite temperature.—We now proceed to a scaling analysis. Under the scaling transformation $q \to q'/b$, $\omega \to \omega'/b^z$, $z = 3$, the parameters involved here scale as $\delta' = \delta b^2$, $\gamma_L' = \gamma_L b^{-2}$ and $u' = u b^{4-d-z}$. Obviously, $4 - (d + z) < 0$ in 3D and u is always irrelevant. This convinces us the Stoner instability at quadratic level. The parameter γ_L is irrelevant, which recovers the scaling of the frequency of longitudinal mode with the dynamical exponent $z_L = 2$. For simplicity, we take the initial value $\alpha_L = \gamma_L = 1$.

Then, we consider the one-loop level correction to the scaling equation. Although the critical fluctuations are anisotropic in momentum space, the RG equations are shown to be closed. Because u is always irrelevant, we linearize the RG equations in u. We obtain the renormalized parameters as: $T(b) = Tb^3$, $\gamma_L(b) = \gamma_L b^{-2}$, $u(b) = ub^{-2}$, and

$$\delta(b) = b^2[\delta + 2u \int_0^{\ln b} dx e^{-(1+z_T)x} f_T^{(2)}(Te^{z_T x}) + u \int_0^{\ln b} dx e^{-(1+z_L)x} f_L^{(2)}(Te^{z_L x})]. \quad (4)$$

The same as traditional Fermi gas, $f_T^{(2)}(t) \simeq f_T^{(2)}(0) + \mathcal{B}_T t^2$ when $t \ll 1$, and is approximately proportional to t when $t > 1$. $f_L^{(2)}(t)$ behaves similarly except the temperature dependence is exponentially small for $t \ll 1$.

We solve the RG equations to $\delta(b_*) = 1$, where the critical fluctuation is weak. If the renormalized temperature $Tb_*^{z_T}, Tb_*^{z_L} \ll 1$, the system stays in the quantum regime as shown by regime I in Fig. 2. We has $\delta(b) = b^2(r + u\mathcal{B}_T T^2/r)$ with $r = \delta - \delta_c$, which displays the Fermi liquid behavior. The correlation length of order parameter correlation is $\xi^{-1/\nu} = r + u\mathcal{B}_T T^2/r$ with $\nu = 1/2$. Self-consistently, we have $T \ll r^{z_T \nu} = r^{3/2}$ for this regime. We find the characteristic quantum fluctuation energy $\hbar\xi^{-z_T}$ and $\hbar\xi^{-z_L}$ is much smaller than the thermal fluctuation energy $k_B T$.

In reigme II, $r^{3/2} \ll T \ll r$, the transverse modes become classical while the longitudinal mode is still quantum-like. The leading temperature dependence of $\delta(b)$ would be $2u\mathcal{C}_T T^{4/3}$, which is is negligible compared with the leading term r. The correlation length is still given by $\xi = r^{-1/2}$.

In regime III and IV, $T \gg r$, both the transverse and the longitudinal mode behaves classically. Except the transverse mode, $\delta(b)$ also obtains contribution from longitudinal mode $u\mathcal{C}_L T^{3/2}$, which is subleading compared to the transverse mode due to $z_L < z_T$. So, correlation length is dominated by the transverse mode: $\xi^{-2} = r + 2u\mathcal{C}_T T^{4/3}$. Comparing the values of r and $2u\mathcal{C}_T T^{4/3}$, we obtain two subregimes: III and IV as shown in Fig. 2. The finite temperature RG also predicts the finite temperature transition boundary: $T_c(r, u) = (-r/2u\mathcal{C}_T)^{3/4}$. Within a narrow window close to $T_c(r, u)$, the system is controlled by the Wilson-Fisher fixed point.

The thermal properties of transverse fluctuations are the same as traditional Fermi liquid [40]. Here we study the longitudinal mode, whose free energy density is given by a universal function $F(r, T) = T^{5/2}\Phi(\frac{r}{T})$ [44]. In the quantum regime of longitudinal mode I/II, $T/r \ll 1$, we obtain the specific-heat coefficient $\gamma = C_V/T$ as $\gamma_q = \frac{A_1}{r^{3/2}} T^2$, where $A_1 \simeq 1.316$. While in classical regime III and IV, $T/r \gg 1$, we have $\gamma_c = A_2 T^{1/2}$, where $A_2 \simeq 0.113$. The behavior of longitudinal mode is similar as anti-ferromagnetic critical point.

Properties in the ordered side.— For $g > g_c$, the order parameter obtains a finite vacuum average value: $\langle\vec{\phi}\rangle = -\frac{g}{2}\langle\vec{M}\rangle$, i.e., ferromagnetic ground state. We find $M \sim (g - g_c)^{1/2}$ from the self-consistent equation, with the same critical exponent as the traditional case. The presence of magnetic order breaks the original symmetry to $[SO(2)_{orbit} \times U(1)_{symmetry}]_D$. The fermionic spectrum as shown in Fig. 3 (a)-(c) is given by

$$\xi_{\mathbf{k},s} = k_\perp^2 + k_z^2 + 2s\sqrt{k_\perp^2 + (k_z - \zeta)^2}, \quad (5)$$

where $k_\perp = \sqrt{k_x^2 + k_y^2}$. We have assumed the magnetization along z direction and taken the units: momentum $k_R = m\lambda$, energy $E_R = k_R^2/2m$. The dimensionless value $\zeta = \frac{Mg}{4\lambda k_R}$ is the crossing point of the spectrum, which denotes the strength of magnetization. The spectrum has a global minimum at $\mathbf{k} = -1\hat{e}_z$, independent to the value of ζ. For non-zero ζ, the ground state obtains a non-zero total momentum as shown in Fig. 3. However, the local current density vanishes due to the presence of vector gauge field (SOC) [41]. The symmetry breaking leads to two pseudo-Goldstone modes, which are transverse spin fluctuations, due to the non-zero momentum. In Fig. 3 (d)-(f), we show the evolution of the Fermi surface for given particle density with increasing magnetization. There is a topological change of the Fermi surface at some intermediate ζ, which gives rise to a Lifshitz transition [42].

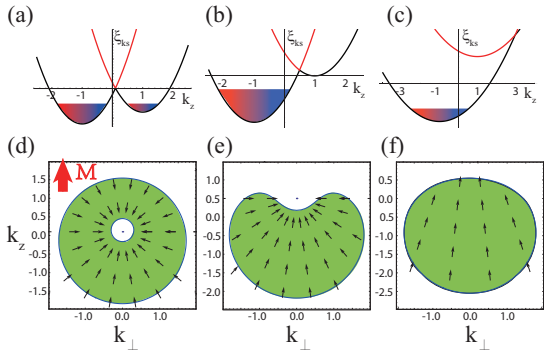

FIG. 3. (Color online) Evolution of fermionic spectrum $\xi_{\mathbf{k}s}$ (upper panel) and Fermi sea (down panel) with increasing magnetization strength ζ. The spectrum has a rotational symmetry about k_z axes. The black arrows show the spin polarization. Parameters taken here are: $\zeta = 0.1$ for (a),(d), $\zeta = 0.5$ for (b),(e), $\zeta = 3$ for (c),(f), SOC strength $\gamma = 0.74$.

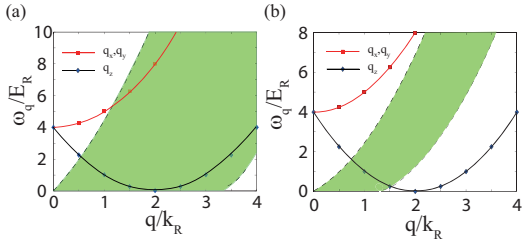

FIG. 4. (Color online) Particle-hole excitation along q_z direction (green regimes) and collective modes for near saturation case $\zeta \gg 1$. (a) plots dense density case and (b) plots dilute density case.

By contrast to traditional Fermi gas, the SOC Fermi gas is more "ordered" in the disordered side: all the spin distributes along the momentum. The magnetic order leads to a shift of the center of spin polarization continuously. Therefore the changes of collective modes is quantitatively small [43]. There are still one gapless mode and three gapped modes across the critical point. However, due to the change of symmetry, the energy gaps of the transverse modes are different from that of longitudinal one ($\Delta_L > \Delta_T$), and the dispersion near $\mathbf{q} = 0$ is linear along q_z direction. The velocity of sound mode is anisotropic: $\omega = v(\theta)q$. With increasing magnetization, the spin polarization changes as shown by arrows in Fig. 3 (d)-(f), and the linear mode and the parallel spin ($\vec{s} \cdot \hat{M}$) are damped due to their strong correlation at intermediate ζ.

The exact analytic solution to this problem seems impossible due to the complex Fermi surface, structure of spin polarization and fermionic spectrum. This problem can be simplified in the limit $\zeta \to \infty$. The fermionic spectrum reduces to $\xi_{\mathbf{k},s} = (\mathbf{k} - s\hat{e}_z)^2 - 2s\zeta - 1$, $s = \pm 1$. Now, the magnetization saturates and only the $s = -1$ band is occupied. The influence of SOC is just a shift of the momentum for upper and lower spectrum. We obtain two gapped pseudo-Goldstone modes corresponding to transverse spin fluctuations, with energy gap about $4E_R$ at $\mathbf{q} = 0$, and has a roton minimum at $\mathbf{q} = 2\hat{e}_z$: $\omega_{\mathbf{q}} = D(\mathbf{q} - 2\hat{e}_z)^2$. Near saturation limit, the dispersion obtains a small imaginary part within the intraband particle-hole excitation (p-h) as shown in Fig. 4. And the roton mode obtains a tiny energy gap.

For intermediate $\zeta \sim \mathcal{O}(1)$, the roton mode will be unstable due to the decay through intra-band p-h excitation for dense density case (Fig. 4 (a)). While for dilute case (Fig. 4 (b)), the roton mode lies outside the p-h continuum. We numerically find the roton mode obtains a negative gap, which vanishes in the dilute limit $\rho \to 0$. Near critical point, $\zeta \to 0$, this roton mode is always covered by p-h continuum because of the difference of Fermi surface in topology as shown in Fig. 3. Therefore, the dilute repulsive SOC Fermi gas might have new phases due to this roton mode after topological change of Fermi surface and deserves further studies in future.

Discussion and summaries.—The 1D SOC has been realized in experiment [12, 13], and simplified proposals for constructing arbitrary types of SOC, which relies on a sequence of pulsed inhomogeneous magnetic fields imprinting suitable phase gradients on the atoms, have been investigated [22–24]. This scheme applies to any atomic species containing arbitrary non-zero spin, for example, ^{6}Li system with hyperfine sublevels $|1/2, -1/2\rangle$ and $|1/2, 1/2\rangle$ chosen as two spin-1/2 states. For ^{6}Li atoms with $N \sim 10^4$ in an isotropic trap with trap frequencies $2\pi \times 10$Hz, and magnetic field gradient strength $\nabla B = 0.09G/\mu$m (within practical range [45]), we estimate the critical interaction strength as $k_F a_s \simeq 0.19$, which is significantly lowered compared to the value π without SOC. Near the critical point, monitoring of spin fluctuations using speckle imaging could provide evidence of formation of magnetic domains [33, 36]. From high resolution density image of the density profile in a trap at finite temperature, one can also extract information about their critical behaviors [37–39].

In summary, we studied itinerant ferromagnetism of 3D repulsive Fermi gas with isotropic SOC. The results here indicate that the presence of large SOC can significantly enhance the magnetization, which makes the realization of itinerant ferromagnetism in experiment more promising. This work reveals rich physics of repulsive SOC Fermi gas across the ferromagnetic phase transition, which provides essentially new picture due to SOC compared to ordinary Fermi gas. This work can be straightforwardly generalized to Rashba or equal weight combination of Rashba and Dresselhaus SOC cases.

This work was supported by the NKBRSFC under grants Nos. 2011CB921502, 2012CB821305, NSFC under grants Nos. 61227902, 61378017, 11311120053. J. Ye

was supported by NSF-DMR-1161497, NSFC-11074173, 11174210, Beijing Municipal Commission of Education under Grant No. PHR201107121, at KITP was supported in part by the NSF under grant No. PHY11-25915.

[1] J. Dalibard, F. Gerbier, G. Juzeliūnas, and P. Öhberg, Rev. Mod. Phys. **83**, 1523 (2011).
[2] I. Bloch, Nat. Phys. **1**, 23 (2005).
[3] M. Lewenstein and W. V. Liu, Nat. Phys. **7**, 101 (2011).
[4] C. L. Kane and E. J. Mele, Phys. Rev. Lett. **95**, 226801 (2005).
[5] B. A. Bernevig, T. L. Hughes, and S. C. Zhang, Science **314**, 1757 (2006).
[6] M. Z. Hasan and C. L. Kane, Rev. Mod. Phys. **82**, 3045 (2010).
[7] X. L. Qi and S. C. Zhang, Rev. Mod. Phys. **83**, 1057 (2011).
[8] Z. Qiao, W.-K. Tse, H. Jiang, Y. Yao, and Q. Niu, Phys. Rev. Lett. **107**, 256801 (2011).
[9] J. Dalibard, F. Gerbier, G. Juzeliūnas, and P. Öhberg, Rev. Mod. Phys. **83**, 1523 (2011).
[10] A. M. Dudarev, R. B. Diener, I. Carusotto, and Q. Niu, Phys. Rev. Lett. **92**, 153005 (2004).
[11] Y. J. Lin, K. Jiménez-García, and I. B. Spielman, Nature (London) **471**, 83 (2011).
[12] P. Wang, Z. Q. Yu, Z. Fu, J. Miao, L. Huang, S. Chai, H. Zhai, and J. Zhang, Phys. Rev. Lett. **109**, 095301 (2012).
[13] L. W. Cheuk, A. T. Sommer, Z. Hadzibabic, T. Yefsah, W. S. Bakr, and M. W. Zwierlein, Phys. Rev. Lett. **109**, 095302 (2012).
[14] C. Wang, C. Gao, C. M. Jian, and H. Zhai, Phys. Rev. Lett. **105**, 160403 (2010).
[15] T. -L. Ho and S. Zhang, Phys. Rev. Lett. **107**, 150403 (2011).
[16] Z. Q. Yu and H. Zhai, Phys. Rev. Lett. **107**, 195305 (2011).
[17] R. Liao, Y. Yi-Xiang, and W. -M. Liu, Phys. Rev. Lett. **108**, 080406 (2012).
[18] H. Hu, L. Jiang, X. -J. Liu, and H. Pu, Phys. Rev. Lett. **107**, 195304 (2011).
[19] H. Hu, B. Ramachandhran, H. Pu, and X. -J. Liu, Phys. Rev. Lett. **108**, 010402 (2012).
[20] C. Qu, Z. Zheng, M. Gong, Y. Xu, L. Mao, X. Zou, G. Guo, and C. Zhang, Nat. Commun. **4**, 2710 (2013).
[21] W. Zhang and W. Yi, Nat. Commun. **4**, 2711 (2013).
[22] B. M. Anderson, I. B. Spielman, and G. Juzeliūnas, Phys. Rev. Lett. **111**, 125301 (2013).
[23] Z.-F. Xu, L. You, and M. Ueda, Phys. Rev. A **87**, 063634 (2013).
[24] Z. -F. Xu and L. You, Phys. Rev. A **85**, 043605 (2012).
[25] Y. Li and C. Wu, Phys. Rev. B **87**, 205126 (2012).
[26] S. S. Zhang, X. L. Yu, J. Ye, and W. M. Liu, Phys. Rev. A **87**, 063623 (2013).
[27] C. Wu, J. Zaanen, and S. -C. Zhang, Phys. Rev. Lett. **95**, 247007 (2005).
[28] X. Cui and T.-L. Ho, Phys. Rev. A **89**, 013629 (2004).
[29] P. Massignan, Z. Yu, and G. M. Bruun, Phys. Rev. Lett. **110**, 230401 (2013).
[30] X. Cui and T.-L. Ho, Phys. Rev. A **89**, 023611 (2004).
[31] Y. Li, E. H. Lieb, and C. Wu, arxiv: 1310.4391.
[32] D. Pekker, M. Babadi, R. Sensarma, N. Zinner, L. Pollet, M. W. Zwierlein, and E. Demler, Phys. Rev. Lett. **106**, 050402 (2011).
[33] C. Sanner, E. J. Su, W. Huang, A. Keshet, J. Gillen, and W. Ketterle, Phys. Rev. Lett. **108**, 240404 (2012).
[34] J. A. Hertz, Phys. Rev. B **14**, 1165 (1976).
[35] A. J. Millis, Phys. Rev. B **48**, 7183 (1993).
[36] C. Sanner, E. J. Su, A. Keshet, W. Huang, J. Gillen, R. Gommers, and W. Ketterle, Phys. Rev. Lett. **106**, 010402 (2011).
[37] Q. Zhou, Y. Kato, N. Kawashima, and N. Trivedi, Phys. Rev. Lett. **103**, 085701 (2009).
[38] Y. Shin, C. H. Schunck, A. Schirotzek, and W. Ketterle, Nature (London) **451**, 689 (2007).
[39] N. Gemelke, X. Zhang, C. -L. Huang, and C. Chin, Nature (London) **460**, 995 (2007).
[40] U. Zülicke and A. J. Millis, Phys. Rev. B **51**, 8996 (1995).
[41] The ground state average of the supercurrent is given by: $\mathbf{j} = \mathbf{j}_k + \mathbf{j}_s$ with $\mathbf{j}_k = (2/V)\sum_{\mathbf{k},s} \mathbf{k} n_{\mathbf{k},s}$ and $\mathbf{j}_s = (2/V)\sum_{\mathbf{k},s} \vec{S}_{\mathbf{k},s} n_{\mathbf{k},s}$, where $n_{\mathbf{k},s} = \Theta(\mu - \xi_{\mathbf{k},s})$, $\vec{S}_{\mathbf{k},s} = s(k_x, k_y, k_z - \zeta)/\sqrt{k_x^2 + k_y^2 + (k_z - \zeta)^2}$ is the spin vector for state $|\mathbf{k}, s\rangle$. It is easy to show that $\mathbf{j} = 0$ for $\zeta \to \infty$ and holds for arbitrary ζ and μ through numerical calculation.
[42] I. M. Lifshitz, Sov. Phys. JETP, **11**, 1130 (1960).
[43] In ordinary Fermi gas, the linear gapless density mode vanishes across the ferromagnetic critical point and a quadratic spin mode appears. This is due to the sudden change of the spin polarization after the phase transition, which is in sharp contrast to SOC Fermi gas.
[44] The universal function is defined as: $\Phi(x) = \frac{K_3}{2}\int_0^\infty dt t^{-5/2} \ln[1 - \exp(-\frac{1}{t}\sqrt{1+xt})]$, where $K_3 = 1/2\pi^2$ is an angle integration factor in 3D. The asymptotic form of $\Phi(x)$ in quantum regime I and II, $x \gg 1$, is given by $\Phi(x) \simeq -K_3 C_1/(2x^{3/2})$, where $C_1 \simeq 4.3292$; while in classical regime III and IV, $x \ll 1$, there is $\Phi(x) \simeq -K_3 C_2/2$, where $C_2 \simeq 1.18886$. The irrelevant interaction u provides small corrections near the critical point.
[45] M. Trinker, S. Groth, S. Haslinger, S. Manz, T. Betz, S. Schneider, I. Bar-Joseph, T. Schumm, and J. Schmiedmayer, Appl. Phys. Lett. **92**, 254102 (2008).